Published in final edited form as:
Bioconjug Chem. 2009 May 20; 20(5): 1016–1025. doi:10.1021/bc9000245.

^{18}F, ^{64}Cu, and ^{68}Ga labeled RGD-bombesin heterodimeric peptides for PET imaging of breast cancer

Zhaofei Liu[1,2], **Yongjun Yan**[1], **Shuanglong Liu**[1], **Fan Wang**[2], and **Xiaoyuan Chen**[1,*]

[1] The Molecular Imaging Program at Stanford (MIPS), Department of Radiology, Biophysics, and Bio-X Program, Stanford University School of Medicine, Stanford, California 94305, USA

[2] Medical Isotopes Research Center, Peking University, Beijing, 100191, China

Abstract

Radiolabeled RGD and bombesin (BBN) radiotracers that specifically target integrin $\alpha_v\beta_3$ and gastrin releasing peptide receptor (GRPR) are both promising radiopharmaceuticals for tumor imaging. We recently designed and synthesized a RGD-BBN heterodimeric peptide with both RGD and BBN motifs in one single molecule. The ^{18}F-labeled RGD-BBN heterodimer exhibited dual integrin $\alpha_v\beta_3$ and GRPR targeting in a PC-3 prostate cancer model. In this study we investigated whether radiolabeled RGD-BBN tracers can be used to detect breast cancer by using microPET. Cell binding assay demonstrated that the high GRPR expressing breast cancer cells typically express low to moderate level of integrin $\alpha_v\beta_3$, while high integrin $\alpha_v\beta_3$ expressing breast cancer cells have negligible level of GRPR. We labeled RGD-BBN heterodimer with three positron emitting radionuclides ^{18}F, ^{64}Cu and ^{68}Ga, and investigated the corresponding PET radiotracers in both orthotopic T47D (GRPR$^+$/low integrin $\alpha_v\beta_3$) and MDA-MB-435 (GRPR$^-$/integrin $\alpha_v\beta_3^+$) breast cancer models. The three radiotracers all possessed in vitro dual integrin $\alpha_v\beta_3$ and GRPR binding affinity. The advantages of the RGD-BBN radiotracers over the corresponding BBN analogues are obvious for imaging MDA-MB-435 (GRPR$^-$/integrin $\alpha_v\beta_3^+$) tumor. ^{18}F-FB-PEG$_3$-RGD-BBN showed lower tumor uptake than ^{64}Cu-NOTA-RGD-BBN and ^{68}Ga-NOTA-RGD-BBN but was able to visualize breast cancer tumors with high contrast. Synthesis of ^{64}Cu-NOTA-RGD-BBN and ^{68}Ga-NOTA-RGD-BBN is much faster and easier than ^{18}F-FB-PEG$_3$-RGD-BBN. ^{64}Cu-NOTA-RGD-BBN showed prolonged tumor uptake, but also higher liver retention and kidney uptake than ^{68}Ga-NOTA-RGD-BBN and ^{18}F-FB-PEG$_3$-RGD-BBN. ^{68}Ga-NOTA-RGD-BBN possessed high tumor signals, but also relatively high background uptake as compared with the other two radiotracers. In summary, the prosthetic labeling groups, chelators and isotopes all have profound effect on the tumor targeting efficacy and in vivo kinetics of the RGD-BBN tracers for dual integrin and GRPR recognition. Further development of suitably labeled RGD-BBN tracers for PET imaging of cancer is warranted.

INTRODUCTION

Breast cancer is the most frequently diagnosed malignancy among women in the Western world and the second leading cause of cancer-related deaths in women (1–3). Early detection of the primary breast cancer or its metastases at distant sites remains the best approach for improving the odds of curing or controlling this disease. The receptors overexpressed on the surface of

*Correspondence should be sent to: Xiaoyuan Chen, PhD, The Molecular Imaging Program at Stanford (MIPS), Department of Radiology and Bio-X Program, Stanford University School of Medicine, 1201 Welch Rd, P095, Stanford, CA 94305-5484, USA, Phone: 650-725-0950; Fax: 650-736-7925.

cancer cells or uniquely expressed during the progress of cancer invasion and metastasis represent the promising targets for breast cancer diagnosis or therapy.

Gastrin-releasing peptide receptor (GRPR) is one of the subtypes of the bombesin (BBN) receptors. GRPRs have been found to be massively overexpressed in several types of human cancers, such as lung cancer, colon cancer, gastric cancer, pancreas cancer, breast cancer, and prostate cancer (4,5). In the past decade, various bombesin and analogs were labeled with different isotopes like ^{99m}Tc, ^{111}In, ^{90}Y, ^{64}Cu, ^{177}Lu, ^{18}F or ^{68}Ga and investigated for GRPR-positive tumor targeted imaging and therapy in both animal models and human trails (6–18). Several bombesin related radiotracers were also investigated for breast cancer imaging (9,19, 20).

It is well documented that integrin $\alpha_v\beta_3$ plays an important role in the regulation of tumor growth, angiogenesis, local invasiveness, and metastatic potential (21–23). Integrin $\alpha_v\beta_3$ is upregulated on the activated tumor endothelial cells and also highly expressed on some tumor cells such as glioblastoma, breast and prostate tumors, malignant melanomas, and ovarian carcinomas (24). Radiolabeled RGD (Arg-Gly-Asp) peptides and analogs that specifically target integrin $\alpha_v\beta_3$ have been wildly tested for tumor imaging in pre-clinical and clinical studies (25–32). Most recently, two ^{18}F labeled RGD based tracers studied in breast cancer patients showed promising results (28,33).

For the one target based breast cancer imaging, the cell-surface receptor must be highly expressed in tumors relative to normal tissues, which may not occur during the whole process of tumor development and in all types of breast cancers. It is thus desirable to develop a new type of radiotracers that can target two types of receptors simultaneously, allowing tumor contrast when either or both receptor types are expressed. We recently designed and synthesized a RGD-BBN heterodimeric peptide that containing both the RGD and BBN motifs in one single molecule (Figure 1) (34,35). The ^{18}F labeled RGD-BBN heterodimer exhibited excellent in vivo kinetic and dual GRPR and integrin $\alpha_v\beta_3$-receptor targeting properties in a PC-3 prostate cancer xenograft model. Here, we would like to test whether radiolabeled RGD-BBN heterodimers can be generally used for the diagnosis of breast cancers as well. In this study, we first screened the GRPR and integrin $\alpha_v\beta_3$ expression in various breast cancer cell lines. We found that among all the tested breast tumor cell lines, almost all the GRPR high expressing tumor cells (e.g. BT474 and T47D) have low to moderate level of integrin $\alpha_v\beta_3$, while the high integrin $\alpha_v\beta_3$ expressing tumor cells (e.g. MDA-MB-435 and MDA-MB-231) have low or undetectable level of GRPR. We thus chose two representative breast cancer models T47D (GRPR$^+$/low integrin $\alpha_v\beta_3$) and MDA-MB-435 (GRPR$^-$/integrin $\alpha_v\beta_3^+$) for in vivo test of ^{18}F-FB-PEG$_3$-RGD-BBN, ^{64}Cu-NOTA-RGD-BBN, and ^{68}Ga-NOTA-RGD-BBN (Figure 1).

EXPERIMENTAL PROCEDURES

All commercially obtained chemicals were of analytical grade and used without further purification. *p*-SCN-Bn-NOTA was purchased from Macrocyclics (Dallas, TX). Chelex 100 resin (50–100 mesh) was purchased from Sigma-Aldrich (St. Louis, MO). Water and all buffers were passed through Chelex 100 column before use in ^{64}Cu and ^{68}Ga labeling procedures to ensure that the aqueous buffer is heavy metal-free. The syringe filter, polyethersulfone membranes (pore size, 0.22 μm; diameter, 13 mm) were obtained from Nalge Nunc International (Rochester, NY). The peptides Aca-BBN(7–14) and c(RGDyK) were synthesized by Peptides International (Louisville, KY). RGD-BBN heterodimer and PEG$_3$-Glu-RGD-BBN were synthesized from Aca-BBN and c(RGDyK) as we previously described (35). Na^{125}I was purchased from Perkin-Elmer (Waltham, MA). ^{125}I-[Tyr^4]BBN (2,000 Ci/mmol) was purchased from GE Healthcare (Piscataway, NJ). ^{64}Cu was obtained from University of

Wisconsin (Madison, WI). No-carrier added ^{18}F-F^- was obtained from an in-house cyclotron (GE Healthcare). ^{68}Ga was obtained from a $^{68}Ge/^{68}Ga$ generator (Obninsk, Russia) and eluted with 0.1 N HCl. The reversed-phase high-performance liquid chromatography (HPLC) system was the same as previously reported (27,36). For NOTA conjugates and ^{18}F-labeled peptides purification, a Vydac protein and peptide column (218TP510; 5 μm, 250 × 10 mm) was used with a flow rate of 5 mL/min. For analytical HPLC and ^{64}Cu or ^{68}Ga labeling purification, a Vydac 218TP54 column (5 μm, 250×4.6 mm) was used with a flow rate of 1 mL/min. The mobile phase was changed from 95% solvent A (0.1% trifluoroacetic acid [TFA] in water) and 5% solvent B (0.1% TFA in acetonitrile, [ACN]) (0–2 min) to 35% solvent A and 65% solvent B at 32 min. The UV absorbance was monitored at 218 nm, and the identification of the peptides was confirmed based on the UV spectrum acquired using a photodiode array (PDA) detector. The radioactivity was detected by model 105S single-channel radiation detector (Carroll and Ramsey Associates).

Synthesis of NOTA conjugates

NOTA-BBN and NOTA-RGD-BBN conjugates were prepared as we previously described (37). In brief, a solution of 2 μmol of peptide (BBN or RGD-BBN) was mixed with 6 μmol of *p*-SCN-Bn-NOTA in 0.1 N $NaHCO_3$ solution (pH = 9.0). After stirring at room temperature for 5 h, the NOTA conjugates were isolated by semi-preparative HPLC. The collected fractions were combined and lyophilized to afford the final product as a white powder. NOTA-bombesin (NOTA-BBN) was obtained in 72% yield with 22.1 min retention time on analytical HPLC. MALDI-TOF-MS was m/z 1504.0 for $[MH]^+$ ($C_{69}H_{102}N_{18}O_{16}S_2$, calculated molecular weight 1503.8). NOTA-RGD-BBN was obtained in 52% yield with 20.7 min retention time on analytical HPLC. MALDI-TOF-MS was m/z 2235.3 for $[MH]^+$ ($C_{102}H_{149}N_{27}O_{26}S_2$, calculated molecular weight 2234.6).

^{68}Ga radiolabeling

The ^{68}Ga labeling procedure was conducted according to the methods we previously described (37). Briefly, 5 nmol of NOTA-BBN or NOTA-RGD-BBN peptide was dissolved in 500 μL of 0.1 M sodium acetate buffer and incubated with 4 mCi (148 MBq) of ^{68}Ga for 15 min at 40°C. ^{68}Ga-NOTA-BBN or ^{68}Ga-NOTA-RGD-BBN product was then purified by analytical HPLC, and the radioactive peak containing the desired product was collected. After removal of the solvent by rotary evaporation, the activity was then reconstituted in PBS and passed through a 0.22-μm Millipore filter into a sterile multidose vial for in vitro and in vivo experiments. The labeling was done with 95% decay-corrected yield for NOTA-BBN (Rt = 21.8 min), and 90% for NOTA-RGD-BBN (R_t = 20.3 min).

^{64}Cu radiolabeling

The ^{64}Cu labeling was performed as we previously described (26,38). Briefly, 5 nmol of NOTA-BBN, or NOTA-RGD-BBN dissolved in NaOAc buffer was labeled with 2 mCi (74 MBq) of ^{64}Cu for 15 min at 40 °C. The labeled peptides were then purified by analytical HPLC. The radioactive peak containing the desired product was collected and rotary evaporated to remove the solvent. The products were then formulated in phosphate-buffered saline (PBS), and passed through a 0.22-μm Millipore filter into a sterile multidose vial for in vitro and in vivo experiments. The labeling was done with 94% decay-corrected yield for NOTA-BBN (R_t = 21.4 min), and 92% for NOTA-RGD-BBN (R_t = 20.5 min).

^{18}F-radiolabeling

The detailed labeling procedure was reported previously (35). PEG_3-RGD-BBN or BBN was labeled with ^{18}F using N-succinimidyl-4-^{18}F-fluorobenzoate (^{18}F-SFB) as the synthon. The desired fractions containing ^{18}F-FB-PEG_3-RGD-BBN or ^{18}F-FB-BBN were combined and

rotary evaporated to dryness, respectively. The products were then passed through a 0.22-μm Millipore filter into a sterile multidose vial for in vitro and in vivo experiments.

Cell lines and animal model

The MDA-MB-231, MDA-MB-468, BT-474, BT-20, T47D, MCF-7 and MDA-MB-435 human breast cancer cell lines, U87MG human glioblastoma cell line and PC-3 human prostate carcinoma cell line were all obtained from the American Type Culture Collection (ATCC, Manassas, VA) and maintained under standard conditions according to ATCC. Animal procedures were performed according to a protocol approved by the Stanford University Institutional Animal Care and Use Committee. The MDA-MB-435 tumor model was established by orthotopic injections of 5×10^6 cells into the right mammary fat pad of female athymic nude mice. For T47D tumor model establishment, the female nude mice were first subcutaneously implanted with 60-day release 17β-estradiol pellets (Innovative Research of America, Sarasota, FL) in the left neck. One day after the estradiol implantation, 1×10^7 T47D cells were orthotopically injected into the right mammary fat pad of the nude mice The mice were subjected to microPET studies when the tumor volume reached 100–300 mm^3 (2–3 weeks for MDA-MB-435, and 4–5 weeks for T47D).

$\alpha_v\beta_3$ receptor levels on the various breast cancer cells, respectively. We labeled c(RGDyK) with $Na^{125}I$ and purified it with HPLC according to our previously described method (39)ded in the 96-well multiscreen DV plates (10^6 cells/well) and then incubated with ~30,000 cpm ^{125}I-[Tyr^4]BBN or ^{125}I-c(RGDyK) for 2 h at room temperature with or without excess doses of cold Acta-BBN(7-14) or c(RGDyK) as blocking agents. After washing with PBS, hydrophilic PVDF filters were collected and the radioactivity was determined using a gamma counter (Packard, Meriden, CT). Results were expressed as percent added dose per million cells (%AD/10^6 cells). Experiment was repeated twice with five parallel samples.

The integrin $\alpha_V\beta_3$ receptor-binding affinity of NOTA-RGD-BBN and FB-PEG_3-RGD-BBN was determined by competition binding assay using ^{125}I-c(RGDyK) as the radioligand on integrin $\alpha_V\beta_3$ high-expressing U87MG cells as we previously described (26)ay using ^{125}I-[Tyr^4]BBN as the radioligand on GRPR high-expressing PC-3 cells as we previously described (10)ssion using Graph-Pad Prism (GraphPad Software, Inc.). Experiments were performed twice with triplicate samples.

Immunofluorescent staining

The expression of GRPR, human integrin $\alpha_v\beta_3$ and murine integrin β_3 on T47D and MDA-MB-435 tumor tissues were detected by immunofluorescent staining. Briefly, frozen T47D and MDA-MB-435 tumor slices (5-μm thickness) from the tumor-bearing nude mice were fixed with ice-cold acetone, rinsed with PBS and blocked with 10% goat serum for 30 min at room temperature. The slices were incubated with goat anti-GRPR antibody (1:100; Santa Cruz Biotechnology, Santa Cruz, CA), humanized anti-human integrin $\alpha_v\beta_3$ antibody Abegrin™ (MedImmune, Gathersberg, MD, 20 μg/mL) (40)d with FITC-conjugated donkey anti-goat, Cy3-conjugated donkey anti-human and FITC-conjugated goat anti-hamster secondary antibodies (1:200; Jackson Immuno-Research Laboratories, West Grove, PA), respectively.

Cell uptake studies

The cell uptake studies were performed as we previous described with some modifications (10,34,35)e day before experiment to allow adherence. Cells were incubated with ^{18}F-FB-PEG_3-RGD-BBN, ^{64}Cu-NOTA-RGD-BBN or ^{68}Ga-NOTA-RGD-BBN (~18 kBq/well) at 37° C for 15, 30, 60, and 120 min. Tumor cells were then washed three times with chilled PBS and harvested by trypsinization with 0.25% trypsin/0.02% EDTA (Invitrogen, Carlsbad, CA). The cells suspensions were collected and measured in a γ counter (Packard, Meriden, CT). The cell

uptake was expressed as the percent added dose (%AD) after decay correction. Experiments were performed twice with triplicate wells.

MicroPET imaging

PET scans and image analysis were performed using a microPET R4 rodent model scanner (Siemens Medical Solutions, Malvern, PA) as previously reported (26,27)u-NOTA-RGD-BBN, or ^{68}Ga-NOTA-RGD-BBN into nude mice bearing T47D or MDA-MB-435 tumor xenografts under isoflurane anesthesia. Five-minute static PET images were acquired at 30 min, 1 h, and 2 h time points postinjection (p.i.). Ten-minute static PET images were acquired at 4 h and 24 h p.i. for ^{64}Cu-NOTA-RGD-BBN (n = 4/group). The images were reconstructed by a 2-dimensional ordered-subsets expectation maximum (OSEM) algorithm, and no correction was necessary for attenuation or scatter correction. For control studies, each group of three mouse bearing MDA-MB-435 tumors were injected via tail-vein with 3.7 MBq (100 μCi) of ^{18}F-FB-BBN, ^{64}Cu-NOTA-BBN, or ^{68}Ga-NOTA-BBN. Five-minute static PET scans were then acquired at 30 min p.i. (n = 3/group).

Serum stability and metabolism

^{18}F-FB-PEG$_3$-RGD-BBN, ^{64}Cu-NOTA-RGD-BBN, or ^{68}Ga-NOTA-RGD-BBN was incubated in fetal bovine serum (FBS) for 2 h at room temperature to test the in vitro serum stability. After passing through a 0.22-μm Millipore filter, the samples were analyzed by radio-HPLC. For metabolism studies, female nude mice (n = 2/group) were injected with ^{18}F-FB-PEG$_3$-RGD-BBN, ^{64}Cu-NOTA-RGD-BBN, or ^{68}Ga-NOTA-RGD-BBN at a dose of 7.4 MBq (200 μCi) in 0.2 mL PBS via tail vein. At 60 min p.i., the urine samples were collected and then centrifuged at 8,000 rpm for 5 min. The supernatant was collected, filtered through a 0.22-μm Millipore filter, and then analyzed by radio-HPLC.

Statistical analysis

Quantitative data were expressed as mean ± SD. Means were compared using one-way analysis of variance (ANOVA) and Student's t test. P values < 0.05 were considered statistically significant.

RESULTS

Chemistry and radiochemistry

The NOTA conjugates of BBN and RGD-BBN were analyzed by both HPLC and mass spectroscopy to confirm the identity of the products. The characterizations of ^{18}F-FB-PEG$_3$-RGD-BBN, ^{64}Cu-NOTA-RGD-BBN, and ^{68}Ga-NOTA-RGD-BBN (Figure 1) are listed in Table 1. The decay-corrected labeling yield of ^{18}F-FB-PEG$_3$-RGD-BBN was 40~50% based on ^{18}F-SFB. The decay-corrected labeling yields of ^{64}Cu-NOTA-RGD-BBN and ^{68}Ga-NOTA-RGD-BBN were both higher than 90% under the condition of reaction at 40 °C for 15 min. After the purification with HPLC, the radiochemical purity of each tracer was higher than 98%. The overall preparation time was ~180 min for ^{18}F-FB-PEG$_3$-RGD-BBN starting from ^{18}F-F, ~40 min for ^{64}Cu-NOTA-RGD-BBN from ^{64}CuCl$_2$, and ~45 min for ^{68}Ga-NOTA-RGD-BBN from ^{68}Ga^{3+} elution. The specific activity of ^{64}Cu-NOTA-RGD-BBN and ^{68}Ga-NOTA-RGD-BBN used in the in vitro and in vivo experiments was typically 7.4~14.8 MBq/nmol (0.2~0.4 Ci/μmol) at the end of synthesis.

Receptor binding affinity

The integrin $\alpha_v\beta_3$ receptor-binding affinities of NOTA-RGD-BBN and FB-PEG$_3$-RGD-BBN were determined by performing competitive binding assay with ^{125}I-c(RGDyK) as the radioligand on U87MG tumor cells. The IC$_{50}$ values for NOTA-RGD-BBN and FB-PEG$_3$-

RGD-BBN were 16.15 ± 2.77 nM, and 13.77 ± 1.82 nM, respectively (mean ± SD, n = 3, Table 1). The binding affinities of NOTA-RGD-BBN and FB-PEG_3-RGD-BBN for GRPR were evaluated using GRPR-positive PC-3 cells with ^{125}I-[Tyr^4]BBN as the radioligand. The IC_{50} values were determined to be 92.75 ± 3.53 nM for NOTA-RGD-BBN, and 73.28 ± 1.57 nM for FB-PEG_3-RGD-BBN (mean ± SD, n =3, Table 1). The comparable IC_{50} values from these two sets of experiments suggest that NOTA-RGD-BBN and FB-PEG_3-RGD-BBN possessed comparable integrin $\alpha_v\beta_3$ binding affinities to c(RGDyK) and GRPR receptor-binding affinities to Aca-BBN(7-14).

GRPR and integrin $\alpha_v\beta_3$ expression on breast cancer cells

The expression of GRPR and integrin $\alpha_v\beta_3$ on various breast cancer cells were determined by radioligand receptor-binding assay using ^{125}I-[Tyr^4]BBN and ^{125}I-c(RGDyK) as radioligands, respectively. As shown in Figure 2A, among all the breast cancer cells tested, T47D expressed the highest level of GRPR as the cell binding percentage of ^{125}I-[Tyr^4]BBN was the highest. The binding specificity of ^{125}I-[Tyr^4]BBN with T47D cells was confirmed by blocking study with cold BBN. The expression of integrin $\alpha_v\beta_3$ on the breast cancer cell lines followed the order of MDA-MB-435 > MDA-MB-231 > MDA-MB-468 > T47D > MCF-7 > BT20 > BT474 (Figure 2B). After blocking with cold c(RGDyK), the cell bound ^{125}I-c(RGDyK) all decreased to a background level, indicating the binding of ^{125}I-c(RGDyK) with the tumor cells was integrin $\alpha_v\beta_3$-mediated specific binding.

Immunofluorescent staining

The expression of GRPR and integrin $\alpha_v\beta_3$ in the T47D and MDA-MB-435 tumor tissues was detected by immunofluorescent staining. As shown in Figure 2C, T47D tumor showed strong GRPR staining, while MDA-MB-435 tumor had only weak background staining, which is consistent with the cell-based radioligand study (Figure 2A). Because the anti-integrin $\alpha_v\beta_3$ antibody Abegrin™ we used can only recognize the human integrin $\alpha_v\beta_3$, which does not cross-react with murine integrin $\alpha_v\beta_3$ of the tumor cells. MDA-MB-435 tumor tissue showed much higher human integrin $\alpha_v\beta_3$ expression than T47D tumor tissue. Besides human integrin $\alpha_v\beta_3$ expressed by the tumor cells, the tumors grown in the nude mice also expressed murine integrin $\alpha_v\beta_3$ on the tumor vasculature. As shown in Figure 2C, both T47D and MDA-MB-435 tumors expressed murine integrin β_3, which can also be recognized by RGD.

Cell uptake studies

The cell uptake studies of ^{18}F-FB-PEG_3-RGD-BBN, ^{64}Cu-NOTA-RGD-BBN and ^{68}Ga-NOTA-RGD-BBN were performed on T47D and MDA-MB-435 tumor cells. As shown in Figure 3A–B, all the radiotracers exhibited an increased uptake with time on both tumor cell lines. Generally speaking, the cell uptake levels of the three tracers on the T47D cells were all higher than those on the MDA-MB-435 tumor cells, which may be due to the higher GRPR expression of the T47D cells, and the GRPR is more easily to be internalized into the cells than integrin. For both tumor cells, the uptake of ^{64}Cu-NOTA-RGD-BBN was significantly higher than that of ^{18}F-FB-PEG_3-RGD-BBN and ^{68}Ga-NOTA-RGD-BBN at late time points ($P < 0.05$). For example, the T47D cell uptake value at 120 min was 4.25 ± 0.13 %AD for ^{18}F-FB-PEG_3-RGD-BBN, 5.30 ± 0.53 %AD for ^{64}Cu-NOTA-RGD-BBN, and 2.42 ± 0.23 %AD for ^{68}Ga-NOTA-RGD-BBN, respectively (n = 3).

MicroPET imaging

Representative coronal microPET images of T47D and MDA-MB-435 tumor-bearing mice (n = 4/group) at different times after intravenous injection of 3.7~5.6 MBq (100~150 μCi) of ^{18}F-FB-PEG_3-RGD-BBN, ^{64}Cu-NOTA-RGD-BBN or ^{68}Ga-NOTA-RGD-BBN are shown in Figure 4. The tumors after injection of the radiotracers were all clearly visible with high

contrast to contralateral background at all time points measured begining 30 min. The mice injected with ^{64}Cu-NOTA-RGD-BBN showed higher abdominal activity accumulation than those injected with ^{68}Ga-NOTA-RGD-BBN or ^{18}F-FB-PEG$_3$-RGD-BBN. Prominent uptake of ^{18}F-FB-PEG$_3$-RGD-BBN was observed in the kidneys and urinary bladder at early time points, suggesting that this radiotracer is mainly excreted through the renal route. Quantification of tumor and major organ activity accumulation in the microPET scans was realized by measuring the regions of interest (ROIs) that encompassing the entire organ on the coronal images. The tumor and major organ uptake comparison of ^{18}F-FB-PEG$_3$-RGD-BBN, ^{64}Cu-NOTA-RGD-BBN and ^{68}Ga-NOTA-RGD-BBN are depicted in Figure 5 and Table 2. The T47D and MDA-MB-435 tumor uptake was expressed as the average of each radiotracer in four mice, while the normal organ uptake was expressed as the average of each tracer in 8 mice (4 T47D tumor-bearing mice and 4 MDA-MB-435 tumor-bearing mice per tracer). As shown in Figure 5, for all three radiotracers, the uptake in T47D tumors was higher than that in MDA-MB-435 tumors at any time point examined, which is consistent with the in vitro cell uptake studies. For example, the tumor uptake comparison of ^{18}F-FB-PEG$_3$-RGD-BBN in T47D tumor and MDA-MB-435 was 2.96 ± 0.53 vs. 2.72 ± 0.80, 1.81 ± 0.34 vs. 1.59 ± 0.65 and 0.91 ± 0.12 vs. 0.84 ± 0.22 %ID/g at 30, 60, and 120 min p.i., respectively (Figure 5A–B). The tumor uptake of ^{68}Ga-NOTA-RGD-BBN was higher than that of the ^{18}F- and ^{64}Cu-labeled RGD-BBN radiotracers from 30 to 120 min p.i. and the differences were statistically significant as compared with ^{18}F-FB-PEG$_3$-RGD-BBN at any time tested ($n = 4$, $P < 0.05$). ^{18}F-FB-PEG$_3$-RGD-BBN also showed rapid wash out in the blood and normal organs. As can be seen from Figure 5, the uptake of the ^{18}F-labeled RGD-BBN decreased rapidly with time in the blood, kidneys and liver. The uptake values of ^{18}F-FB-PEG$_3$-RGD-BBN in the blood and normal organs were all significantly lower than those of the ^{64}Cu and ^{68}Ga tracers at any time from 30 to 120 min ($n = 8$, $P < 0.05$). ^{68}Ga-NOTA-RGD-BBN also showed higher blood retention as compared to the ^{18}F and ^{64}Cu radiotracers (Figure 5C). The kidney uptake of ^{68}Ga-NOTA-RGD-BBN and ^{64}Cu-NOTA-RGD-BBN decreased with time and ^{68}Ga-NOTA-RGD-BBN seemed to be cleared slightly more rapidly than ^{64}Cu-NOTA-RGD-BBN. At 120 min p.i., the kidney uptake was 0.74 ± 0.19 %ID/g for ^{18}F-FB-PEG$_3$-RGD-BBN, 1.64 ± 0.40 %ID/g for ^{68}Ga-NOTA-RGD-BBN and 3.28 ± 0.99 %ID/g for ^{64}Cu-NOTA-RGD-BBN, respectively ($n = 8$, Figure 5D). The liver uptake of ^{64}Cu-NOTA-RGD-BBN was significantly higher than those of the ^{18}F- and ^{68}Ga-labeled RGD-BBN radiotracers at any time point examined ($n = 8$, $P < 0.05$). At 4 h and 24 h p.i., the liver uptake of ^{64}Cu-NOTA-RGD-BBN was still higher than that of the tumor uptake (Table 2). The liver uptake of ^{18}F-FB-PEG$_3$-RGD-BBN was very low with the highest uptake being 1.13 ± 0.43 %ID/g at 30 min p.i., indicating that the ^{18}F labeled RGD-BBN was excreted predominantly through the renal route (Figure 5E). Although the absolute tumor uptake of ^{18}F-FB-PEG$_3$-RGD-BBN was lower than that of the other two radiotracers, the tumor-to-nontumor (T/NT) ratios of ^{18}F-FB-PEG$_3$-RGD-BBN were all significantly higher than those of ^{64}Cu-NOTA-RGD-BBN and ^{68}Ga-NOTA-RGD-BBN ($P < 0.05$), due to the rapid washout of the tracer in blood and normal organs (Figure 5F).

MDA-MB-435 tumor is integrin $\alpha_v\beta_3$-positive but GRPR-negative (Figure 2B). As shown in Figure 6A, the BBN radiotracers appeared to be more lipophilic than the corresponding RGD-BBN radiotracers, resulting in significant activity accumulation in the gallbladder and intestines. Due to the absence of GRPR, neither ^{18}F-FB-BBN, ^{64}Cu-NOTA-RGD-BBN nor ^{68}Ga-NOTA-RGD-BBN was able to visualize the tumors. The MDA-MB-435 tumor uptake at 30 min p.i. was 0.45 ± 0.11 %ID/g for ^{18}F-FB-BBN, 0.63 ± 0.17 %ID/g for ^{64}Cu-NOTA-RGD-BBN and 0.57 ± 0.13 %ID/g for ^{68}Ga-NOTA-RGD-BBN, which was significantly lower than the corresponding RGD-BBN radiotracers ($P < 0.01$, Figure 6B).

Serum stability and metabolic stability

The serum stability of ^{18}F-FB-PEG$_3$-RGD-BBN, ^{64}Cu-NOTA-RGD-BBN, and ^{68}Ga-NOTA-RGD-BBN was tested by incubating with FBS for 2 h at room temperature. As shown in Figure 7A, all three radiotracers showed good in vitro serum stability, with only minor peaks (Rt around 5 min) for ^{18}F-FB-PEG$_3$-RGD-BBN and ^{64}Cu-NOTA-RGD-BBN as detected by radio-HPLC. We also studied the metabolic stability of the three radiotracers in mice urine at 60 min after injection. As shown in Figure 7B, all three radiotracers showed detectable metabolites in the urine. Although we did not identify the composition of the metabolites, it was found that all metabolites came off the HPLC column eluted earlier than the parent compounds. The major metabolite peaks were found at about 17 min for ^{68}Ga-NOTA-RGD-BBN and ^{18}F-FB-PEG$_3$-RGD-BBN, and about 20 min for ^{64}Cu-NOTA-RGD-BBN. Because the RGD peptides seemed to be more metabolically stable than BBN peptides in urine (11, 40), we speculate that the metabolites of the RGD-BBN radiotracers were more likely to be from the BBN counterparts of the radiolabeled heterodimers.

DISCUSSION

In this study, we investigated whether radiolabeled RGD-BBN heterodimers can be used as probes for breast cancer PET imaging. The RGD-BBN was labeled with three most commonly used positron emitters (^{18}F, ^{64}Cu, and ^{68}Ga), and the tumor targeting and in vivo kinetics of the corresponding radiotracers were compared in two orthotopic breast cancer models.

Breast cancers can be sorted into two categories, estrogen dependent (ER^+) and estrogen-independent (ER^-), based on the presence or absence of estrogen receptors (41). We screened the GRPR and integrin $\alpha_v\beta_3$ expression in both the ER^+ (T47D, BT474, MCF-7) and ER^- (MDA-MB-231, MDA-MB-435, MDA-MB468, BT20) breast cancer cells (42–45). T47D and BT474 cells had high GRPR but low to moderate integrin $\alpha_v\beta_3$ expression. On the other hand, the estrogen-independent tumor cells such as MDA-MB-435, MDA-MB-231, and MDA-MB-468 had high integrin $\alpha_v\beta_3$, but undetectable GRPR expression (Figure 2A–B). It is of note that MDA-MB-435 cells were reported to express GRPR at mRNA level (43) but our receptor binding assay using ^{125}I-[Tyr^4]BBN indicated low level of GRPR at the protein level. We selected the T47D and MDA-MB-435 tumor cells for further investigation, which represent the two typical types of breast cancers. The tumor tissues were investigated by immunohistochemical staining to confirm the receptor expression. The expression of GRPR and human integrin $\alpha_v\beta_3$ was consistent with the cell binding assay data. Although the tumor cells are of human origin, the tumor endothelial cells are of murine origin, we thus also checked integrin expression on the tumor vasculature murine integirn β_3 staining and found that both T47D and MDA-MB-435 tumor vasculatures were integrin positive (Figure 2C).

The RGD-BBN peptides were labeled with ^{18}F, ^{64}Cu and ^{68}Ga, respectively. ^{18}F labeling of peptides typically require lengthy procedures because ^{18}F-F^- is cyclotron-dependent and a prosthetic group such as ^{18}F-SFB needs to be synthesized before peptide labeling. In contrast, the metal isotopes such as ^{64}Cu and ^{68}Ga can be easily labeled with the chelated RGD-BBN peptides. In particular, ^{68}Ga can be easily acquired from an in-house ^{68}Ge/^{68}Ga generator (^{68}Ge, $t_{1/2}$ = 270.8 days) instead of from a medical cyclotron. All the three radiotracers showed similar dual receptor binding affinity as determined by receptor binding assay, indicating that the radiotracers maintained the comparable in vitro dual receptor-binding properties. Each radiotracer can be acquired in high radiochemical purity after being purified by HPLC, which is sufficient for both in vitro and in vivo experiments. The in vitro cell uptake studies demonstrated that the cell uptake values of the radiotracers on T47D tumor cells were higher than those on MDA-MB-435 tumor cells, which may be caused by the much higher GRPR expression on the T47D cells, leading to efficient internalization of the radiotracers.

The in vivo behaviors of the three radiotracers were tested by microPET in orthotopic T47D and MDA-MB-435 breast cancer models. The radiolabeled BBN was also tested in the non-GRPR expressing MDA-MB-435 tumor model as a control. The much higher tumor uptake of the ^{18}F, ^{64}Cu, and ^{68}Ga labeled RGD-BBN radiotracers than those of the corresponding BBN radiotracers indicates that the RGD-BBN tracers are more useful for imaging than BBN tracers in GRPR negative tumors. We did not compare the tumor imaging characteristics of RGD-BBN and RGD radiotracers in vivo as we were unable to identify a breast cancer model that is completely integrin negative as all the integrin negative tumor cell lines when inoculated into mice develop integrin positive tumor vasculature. The metal isotopes labeled radiotracers showed higher background than ^{18}F tracers, and ^{18}F labeled RGD-BBN showed a more rapid washed out than ^{64}Cu and ^{68}Ga-labeled same peptide. The tumor uptake of ^{18}F-FB-PEG$_3$-RGD-BBN was also found to be lower than that of the ^{64}Cu and ^{68}Ga labeled RGD-BBN radiotracers. The similar trend has been previously found in both BBN and RGD peptide cases (29).

The selection of chelators for radiometal labeling is important. For ^{68}Ga labeling, NOTA is commonly used because the rapid reaction kinetics of NOTA can meet the short half-life of ^{68}Ga ($t_{1/2}$ = 68 min). The NOTA conjugates can reach a higher yield when incubated with ^{68}Ga for 10 min at room temperature (37). For ^{64}Cu labeling, DOTA was previously reported as a widely used “universal” chelator, and we have reported a series of ^{64}Cu-DOTA peptide tracers for tumor imaging (10,26,38,46,47). The high and prolonged liver uptake is problematic for ^{64}Cu-DOTA radiotracers, which was suggested to be the slow dissociation of ^{64}Cu from the DOTA chelator (48–51). The instability of the ^{64}Cu-DOTA conjugates would result in demetallation and subsequent accumulation in nontarget tissues such as the liver (49). Recently, Prasanphanich et al. (49) reported ^{64}Cu-labeled bombesin analogs using NOTA as a chelator. Their results suggested high in vivo kinetic stability of ^{64}Cu-NOTA-BBN vectors with little or no dissociation of ^{64}Cu from NOTA. From the microPET data, the liver uptake of ^{64}Cu-NOTA-RGD-BBN was relatively lower than other ^{64}Cu-DOTA radiotracers (18,26), but still higher than ^{68}Ga-NOTA-RGD-BBN, which may be caused by the ^{68}Ga chelating ability of NOTA is higher than ^{64}Cu (52).

Acknowledgments

This work was supported, in part, by the National Cancer Institute (NCI; R01 120188, R01 CA119053, R21 CA121842, R21 CA102123, P50 CA114747, U54 CA119367, and R24 CA93862). We thank the cyclotron team at Stanford University for ^{18}F-F$^-$ production and thank the cyclotron team of University of Wisconsin-Madison for ^{64}Cu production. Z. Liu acknowledges the China Scholarship Council (CSC) for partly financial support during his study at Stanford University.

Abbreviations

NOTA	1,4,7-triazacyclononane-1,4,7-triacetic acid
GRPR	gastrin-releasing peptide receptor
PEG$_3$	11-amino-3,6,9-trioxaundecanoic acid
Aca-BBN(7-14)	Aca-Gln-Trp-Ala-Val-Gly-His-Leu-Met-NH$_2$
c(RGDyK)	cyclo(Arg-Gly-Asp-D-Tyr-Lys)
RGD-BBN	cyclo(Arg-Gly-Asp-D-Tyr-Lys)-Glu-(Aca-Gln-Trp-Ala-Val-Gly-His-Leu-Met-NH$_2$)
SFB	*N*-succinimidyl-4-fluorobenzoate

LITERATURE CITED

1. Greenlee RT, Hill-Harmon MB, Murray T, Thun M. Cancer statistics, 2001. CA Cancer J Clin 2001;51:15–36. [PubMed: 11577478]
2. Veronesi U, Boyle P, Goldhirsch A, Orecchia R, Viale G. Breast cancer. Lancet 2005;365:1727–41. [PubMed: 15894099]
3. Weigelt B, Peterse JL, van't Veer LJ. Breast cancer metastasis: markers and models. Nat Rev Cancer 2005;5:591–602. [PubMed: 16056258]
4. Cornelio DB, Roesler R, Schwartsmann G. Gastrin-releasing peptide receptor as a molecular target in experimental anticancer therapy. Ann Oncol 2007;18:1457–66. [PubMed: 17351255]
5. Smith CJ, Volkert WA, Hoffman TJ. Radiolabeled peptide conjugates for targeting of the bombesin receptor superfamily subtypes. Nucl Med Biol 2005;32:733–40. [PubMed: 16243649]
6. Schweinsberg C, Maes V, Brans L, Blauenstein P, Tourwe DA, Schubiger PA, Schibli R, Garayoa EG. Novel glycated [^{99m}Tc(CO)$_3$]-labeled bombesin analogues for improved targeting of gastrin-releasing peptide receptor-positive tumors. Bioconjug Chem 2008;19:2432–9. [PubMed: 19053304]
7. Santos-Cuevas CL, Ferro-Flores G, Arteaga de Murphy C, Pichardo-Romero PA. Targeted imaging of gastrin-releasing peptide receptors with ^{99m}Tc-EDDA/HYNIC-[Lys^3]-bombesin: biokinetics and dosimetry in women. Nucl Med Commun 2008;29:741–7. [PubMed: 18753829]
8. Garrison JC, Rold TL, Sieckman GL, Naz F, Sublett SV, Figueroa SD, Volkert WA, Hoffman TJ. Evaluation of the pharmacokinetic effects of various linking group using the ^{111}In-DOTA-X-BBN (7-14)NH$_2$ structural paradigm in a prostate cancer model. Bioconjug Chem 2008;19:1803–12. [PubMed: 18712899]
9. Van de Wiele C, Phonteyne P, Pauwels P, Goethals I, Van den Broecke R, Cocquyt V, Dierckx RA. Gastrin-releasing peptide receptor imaging in human breast carcinoma versus immunohistochemistry. J Nucl Med 2008;49:260–4. [PubMed: 18199617]
10. Chen X, Park R, Hou Y, Tohme M, Shahinian AH, Bading JR, Conti PS. microPET and autoradiographic imaging of GRP receptor expression with ^{64}Cu-DOTA-[Lys^3]bombesin in human prostate adenocarcinoma xenografts. J Nucl Med 2004;45:1390–7. [PubMed: 15299066]
11. Zhang X, Cai W, Cao F, Schreibmann E, Wu Y, Wu JC, Xing L, Chen X. ^{18}F-labeled bombesin analogs for targeting GRP receptor-expressing prostate cancer. J Nucl Med 2006;47:492–501. [PubMed: 16513619]
12. Dimitrakopoulou-Strauss A, Hohenberger P, Haberkorn U, Macke HR, Eisenhut M, Strauss LG. ^{68}Ga-labeled bombesin studies in patients with gastrointestinal stromal tumors: comparison with ^{18}F-FDG. J Nucl Med 2007;48:1245–50. [PubMed: 17631559]
13. Schuhmacher J, Zhang H, Doll J, Macke HR, Matys R, Hauser H, Henze M, Haberkorn U, Eisenhut M. GRP receptor-targeted PET of a rat pancreas carcinoma xenograft in nude mice with a ^{68}Ga-labeled bombesin(6-14) analog. J Nucl Med 2005;46:691–9. [PubMed: 15809493]
14. Waser B, Eltschinger V, Linder K, Nunn A, Reubi JC. Selective in vitro targeting of GRP and NMB receptors in human tumours with the new bombesin tracer ^{177}Lu-AMBA. Eur J Nucl Med Mol Imaging 2007;34:95–100. [PubMed: 16909223]
15. Lantry LE, Cappelletti E, Maddalena ME, Fox JS, Feng W, Chen J, Thomas R, Eaton SM, Bogdan NJ, Arunachalam T, Reubi JC, Raju N, Metcalfe EC, Lattuada L, Linder KE, Swenson RE, Tweedle MF, Nunn AD. ^{177}Lu-AMBA: Synthesis and characterization of a selective ^{177}Lu-labeled GRP-R agonist for systemic radiotherapy of prostate cancer. J Nucl Med 2006;47:1144–52. [PubMed: 16818949]
16. Zhang H, Chen J, Waldherr C, Hinni K, Waser B, Reubi JC, Maecke HR. Synthesis and evaluation of bombesin derivatives on the basis of pan-bombesin peptides labeled with indium-111, lutetium-177, and yttrium-90 for targeting bombesin receptor-expressing tumors. Cancer Res 2004;64:6707–15. [PubMed: 15374988]
17. Cai W, Shin DW, Chen K, Gheysens O, Cao Q, Wang SX, Gambhir SS, Chen X. Peptide-labeled near-infrared quantum dots for imaging tumor vasculature in living subjects. Nano Lett 2006;6:669–76. [PubMed: 16608262]

18. Yang YS, Zhang X, Xiong Z, Chen X. Comparative in vitro and in vivo evaluation of two ^{64}Cu-labeled bombesin analogs in a mouse model of human prostate adenocarcinoma. Nucl Med Biol 2006;33:371–80. [PubMed: 16631086]
19. Scopinaro F, Varvarigou AD, Ussof W, De Vincentis G, Sourlingas TG, Evangelatos GP, Datsteris J, Archimandritis SC. Technetium labeled bombesin-like peptide: preliminary report on breast cancer uptake in patients. Cancer Biother Radiopharm 2002;17:327–35. [PubMed: 12136525]
20. Parry JJ, Andrews R, Rogers BE. MicroPET imaging of breast cancer using radiolabeled bombesin analogs targeting the gastrin-releasing peptide receptor. Breast Cancer Res Treat 2007;101:175–83. [PubMed: 16838112]
21. Hood JD, Cheresh DA. Role of integrins in cell invasion and migration. Nat Rev Cancer 2002;2:91–100. [PubMed: 12635172]
22. Ruoslahti E. Specialization of tumour vasculature. Nat Rev Cancer 2002;2:83–90. [PubMed: 12635171]
23. Brooks PC, Clark RA, Cheresh DA. Requirement of vascular integrin αvβ3 for angiogenesis. Science 1994;264:569–71. [PubMed: 7512751]
24. Hynes RO. Integrins: bidirectional, allosteric signaling machines. Cell 2002;110:673–87. [PubMed: 12297042]
25. Chen X, Park R, Shahinian AH, Tohme M, Khankaldyyan V, Bozorgzadeh MH, Bading JR, Moats R, Laug WE, Conti PS. ^{18}F-labeled RGD peptide: initial evaluation for imaging brain tumor angiogenesis. Nucl Med Biol 2004;31:179–89. [PubMed: 15013483]
26. Wu Y, Zhang X, Xiong Z, Cheng Z, Fisher DR, Liu S, Gambhir SS, Chen X. microPET imaging of glioma integrin αvβ3 expression using ^{64}Cu-labeled tetrameric RGD peptide. J Nucl Med 2005;46:1707–18. [PubMed: 16204722]
27. Zhang X, Xiong Z, Wu Y, Cai W, Tseng JR, Gambhir SS, Chen X. Quantitative PET imaging of tumor integrin αvβ3 expression with ^{18}F-FRGD2. J Nucl Med 2006;47:113–21. [PubMed: 16391195]
28. Beer AJ, Niemeyer M, Carlsen J, Sarbia M, Nahrig J, Watzlowik P, Wester HJ, Harbeck N, Schwaiger M. Patterns of αvβ3 expression in primary and metastatic human breast cancer as shown by ^{18}F-Galacto-RGD PET. J Nucl Med 2008;49:255–9. [PubMed: 18199623]
29. Decristoforo C, Hernandez Gonzalez I, Carlsen J, Rupprich M, Huisman M, Virgolini I, Wester HJ, Haubner R. ^{68}Ga- and ^{111}In-labelled DOTA-RGD peptides for imaging of αvβ3 integrin expression. Eur J Nucl Med Mol Imaging 2008;35:1507–15. [PubMed: 18369617]
30. Cai W, Niu G, Chen X. Imaging of integrins as biomarkers for tumor angiogenesis. Curr Pharm Des 2008;14:2943–73. [PubMed: 18991712]
31. Cai W, Chen X. Multimodality molecular imaging of tumor angiogenesis. J Nucl Med 2008;49(Suppl 2):113S–28S. [PubMed: 18523069]
32. Chen X. Multimodality imaging of tumor integrin αvβ3 expression. Mini Rev Med Chem 2006;6:227–34. [PubMed: 16472190]
33. Kenny LM, Coombes RC, Oulie I, Contractor KB, Miller M, Spinks TJ, McParland B, Cohen PS, Hui AM, Palmieri C, Osman S, Glaser M, Turton D, Al-Nahhas A, Aboagye EO. Phase I trial of the positron-emitting Arg-Gly-Asp (RGD) peptide radioligand ^{18}F-AH111585 in breast cancer patients. J Nucl Med 2008;49:879–86. [PubMed: 18483090]
34. Li ZB, Wu Z, Chen K, Ryu EK, Chen X. ^{18}F-labeled BBN-RGD heterodimer for prostate cancer imaging. J Nucl Med 2008;49:453–61. [PubMed: 18287274]
35. Liu Z, Yan Y, Chin FT, Wang F, Chen X. Dual integrin and gastrin-releasing peptide receptor targeted tumor imaging using ^{18}F-labeled PEGylated RGD-bombesin heterodimer ^{18}F-FB-PEG$_3$-Glu-RGD-BBN. J Med Chem 2009;52:425–32. [PubMed: 19113865]
36. Cai W, Zhang X, Wu Y, Chen X. A thiol-reactive ^{18}F-labeling agent, N-[2-(4-^{18}F-fluorobenzamido) ethyl]maleimide, and synthesis of RGD peptide-based tracer for PET imaging of αvβ3 integrin expression. J Nucl Med 2006;47:1172–80. [PubMed: 16818952]
37. Li ZB, Chen K, Chen X. ^{68}Ga-labeled multimeric RGD peptides for microPET imaging of integrin αvβ3 expression. Eur J Nucl Med Mol Imaging 2008;35:1100–8. [PubMed: 18204838]

38. Li ZB, Cai W, Cao Q, Chen K, Wu Z, He L, Chen X. ^{64}Cu-labeled tetrameric and octameric RGD peptides for small-animal PET of tumor αvβ3 integrin expression. J Nucl Med 2007;48:1162–71. [PubMed: 17574975]
39. Chen X, Park R, Shahinian AH, Bading JR, Conti PS. Pharmacokinetics and tumor retention of ^{125}I-labeled RGD peptide are improved by PEGylation. Nucl Med Biol 2004;31:11–9. [PubMed: 14741566]
40. Wu Z, Li ZB, Cai W, He L, Chin FT, Li F, Chen X. ^{18}F-labeled mini-PEG spacered RGD dimer (^{18}F-FPRGD2): synthesis and microPET imaging of αvβ3 integrin expression. Eur J Nucl Med Mol Imaging 2007;34:1823–31. [PubMed: 17492285]
41. Vaïk Strande, Canelle L, Tastet C, Burlet-Schiltz O, Monsarrat B, Hondermarck H. The proteome of the human breast cancer cell line MDA-MB-231: Analysis by LTQ-Orbitrap mass spectrometry. Proteomics Clin Appl 2009;3:41–50.
42. Cassoni P, Papotti M, Ghe C, Catapano F, Sapino A, Graziani A, Deghenghi R, Reissmann T, Ghigo E, Muccioli G. Identification, characterization, and biological activity of specific receptors for natural (ghrelin) and synthetic growth hormone secretagogues and analogs in human breast carcinomas and cell lines. J Clin Endocrinol Metab 2001;86:1738–45. [PubMed: 11297611]
43. Bajo AM, Schally AV, Krupa M, Hebert F, Groot K, Szepeshazi K. Bombesin antagonists inhibit growth of MDA-MB-435 estrogen-independent breast cancers and decrease the expression of the ErbB-2/HER-2 oncoprotein and c-jun and c-fos oncogenes. Proc Natl Acad Sci U S A 2002;99:3836–41. [PubMed: 11891317]
44. Anzick SL, Kononen J, Walker RL, Azorsa DO, Tanner MM, Guan XY, Sauter G, Kallioniemi OP, Trent JM, Meltzer PS. AIB1, a Steroid Receptor Coactivator Amplified in Breast and Ovarian Cancer. Science 1997;277:965–968. [PubMed: 9252329]
45. Brandi G, Paiardini M, Cervasi B, Fiorucci C, Filippone P, De Marco C, Zaffaroni N, Magnani M. A new indole-3-carbinol tetrameric derivative inhibits cyclin-dependent kinase 6 expression, and induces G1 cell cycle arrest in both estrogen-dependent and estrogen-independent breast cancer cell lines. Cancer Res 2003;63:4028–36. [PubMed: 12874002]
46. Cai W, Wu Y, Chen K, Cao Q, Tice DA, Chen X. In vitro and in vivo characterization of ^{64}Cu-labeled Abegrin, a humanized monoclonal antibody against integrin alpha v beta 3. Cancer Res 2006;66:9673–81. [PubMed: 17018625]
47. Chen X, Liu S, Hou Y, Tohme M, Park R, Bading JR, Conti PS. MicroPET imaging of breast cancer alphav-integrin expression with ^{64}Cu-labeled dimeric RGD peptides. Mol Imaging Biol 2004;6:350–9. [PubMed: 15380745]
48. Wadas TJ, Eiblmaier M, Zheleznyak A, Sherman CD, Ferdani R, Liang K, Achilefu S, Anderson CJ. Preparation and biological evaluation of ^{64}Cu-CB-TE2A-sst2-ANT, a somatostatin antagonist for PET imaging of somatostatin receptor-positive tumors. J Nucl Med 2008;49:1819–27. [PubMed: 18927338]
49. Prasanphanich AF, Nanda PK, Rold TL, Ma L, Lewis MR, Garrison JC, Hoffman TJ, Sieckman GL, Figueroa SD, Smith CJ. [^{64}Cu-NOTA-8-Aoc-BBN(7-14)NH_2] targeting vector for positron-emission tomography imaging of gastrin-releasing peptide receptor-expressing tissues. Proc Natl Acad Sci U S A 2007;104:12462–7. [PubMed: 17626788]
50. Boswell CA, Sun X, Niu W, Weisman GR, Wong EH, Rheingold AL, Anderson CJ. Comparative in vivo stability of copper-64-labeled cross-bridged and conventional tetraazamacrocyclic complexes. J Med Chem 2004;47:1465–74. [PubMed: 14998334]
51. Garrison JC, Rold TL, Sieckman GL, Figueroa SD, Volkert WA, Jurisson SS, Hoffman TJ. In vivo evaluation and small-animal PET/CT of a prostate cancer mouse model using ^{64}Cu bombesin analogs: side-by-side comparison of the CB-TE2A and DOTA chelation systems. J Nucl Med 2007;48:1327–37. [PubMed: 17631556]
52. Clarke E, Martell AE. Stabilities of the Fe(III), Ga(III) and In(III) chelates of N,N′,N″-triazacyclononanetriacetic acid. Inorg Chim Acta 1991;181:273–80.

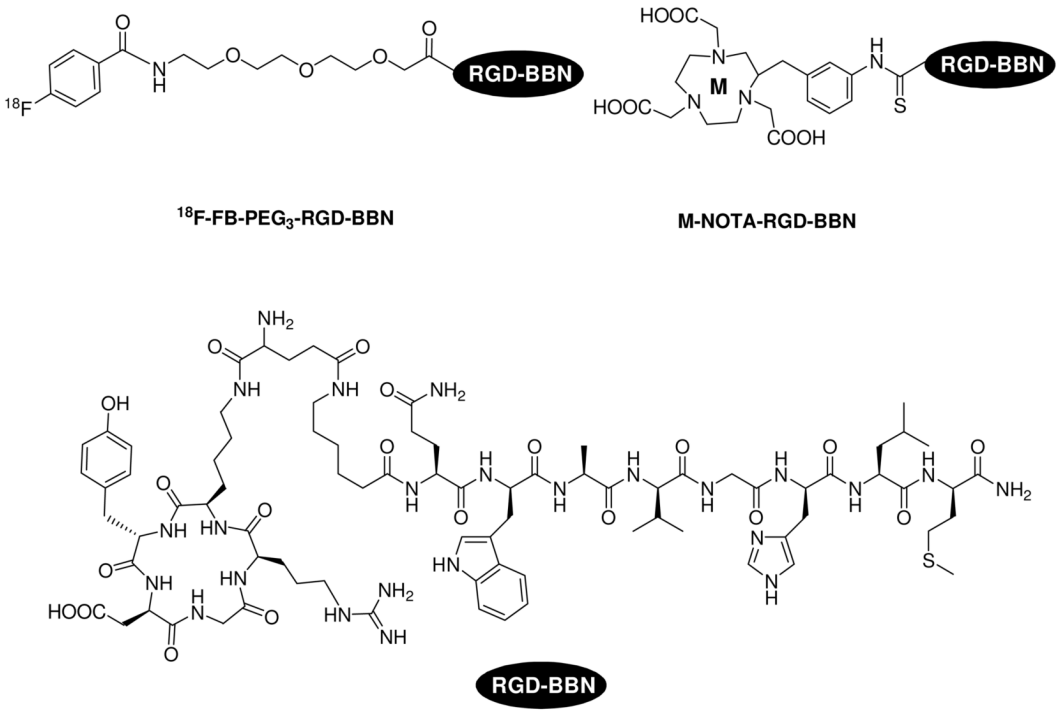

Figure 1.

Chemical structures of ^{18}F-FB-PEG$_3$-RGD-BBN and NOTA-RGD-BBN with M corresponding to the chelated ^{64}Cu or ^{68}Ga. RGD-BBN: cyclo(Arg-Gly-Asp-D-Tyr-Lys)-Glu-(Aca-Gln-Trp-Ala-Val-Gly-His-Leu-Met-NH$_2$).

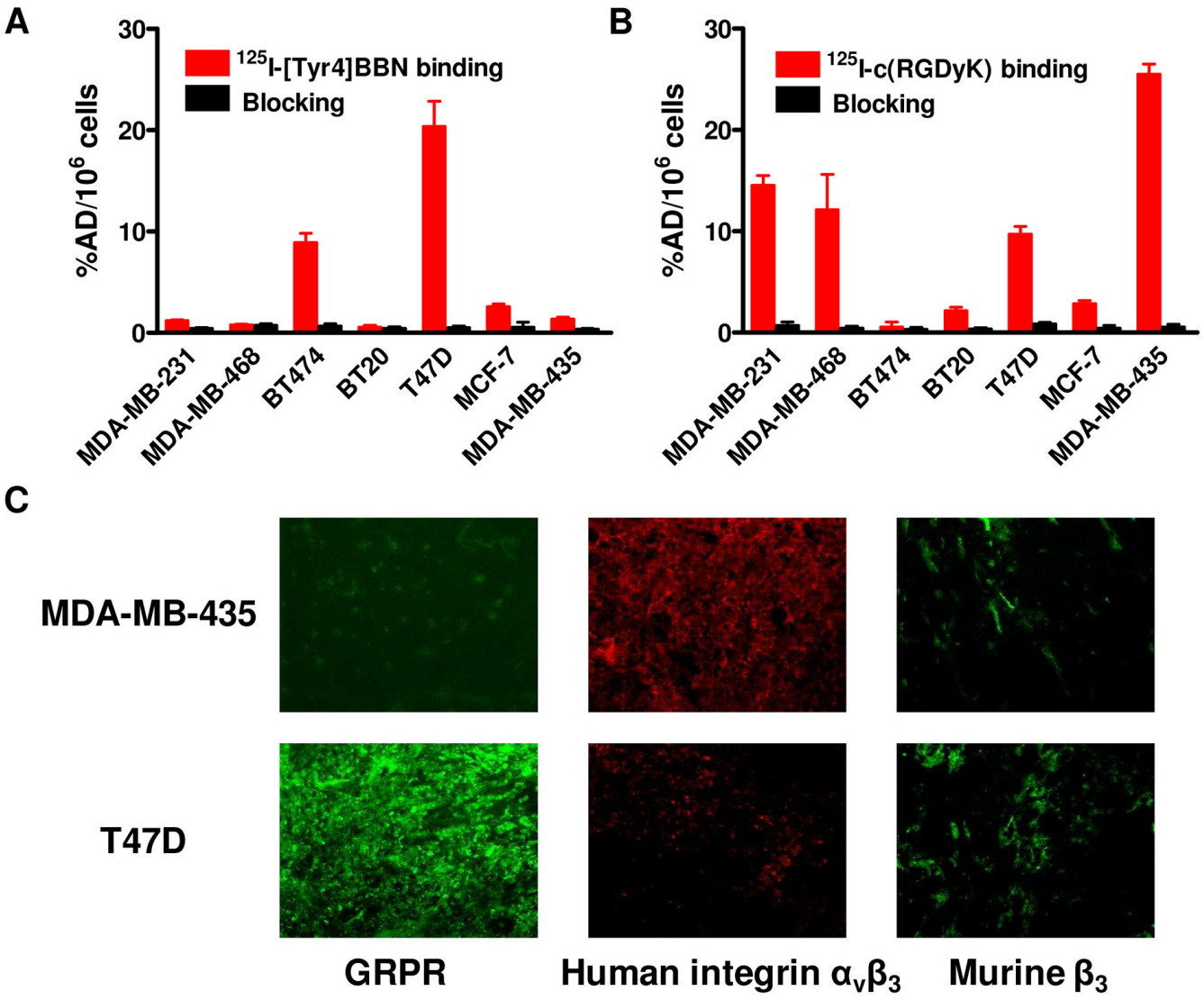

Figure 2.

(A–B) GRPR and integrin $\alpha_v\beta_3$ levels in different breast cancer cell lines determined by cell binding assay using ^{125}I-[Tyr^4]BBN (A) or ^{125}I-c(RGDyK) (B) as the radioligand (means ± SD, n = 5). (C) Immunofluorescent staining for GRPR, human integrin $\alpha_v\beta_3$ and murine integrin β_3 in MDA-MB-435 and T47D tumor tissues.

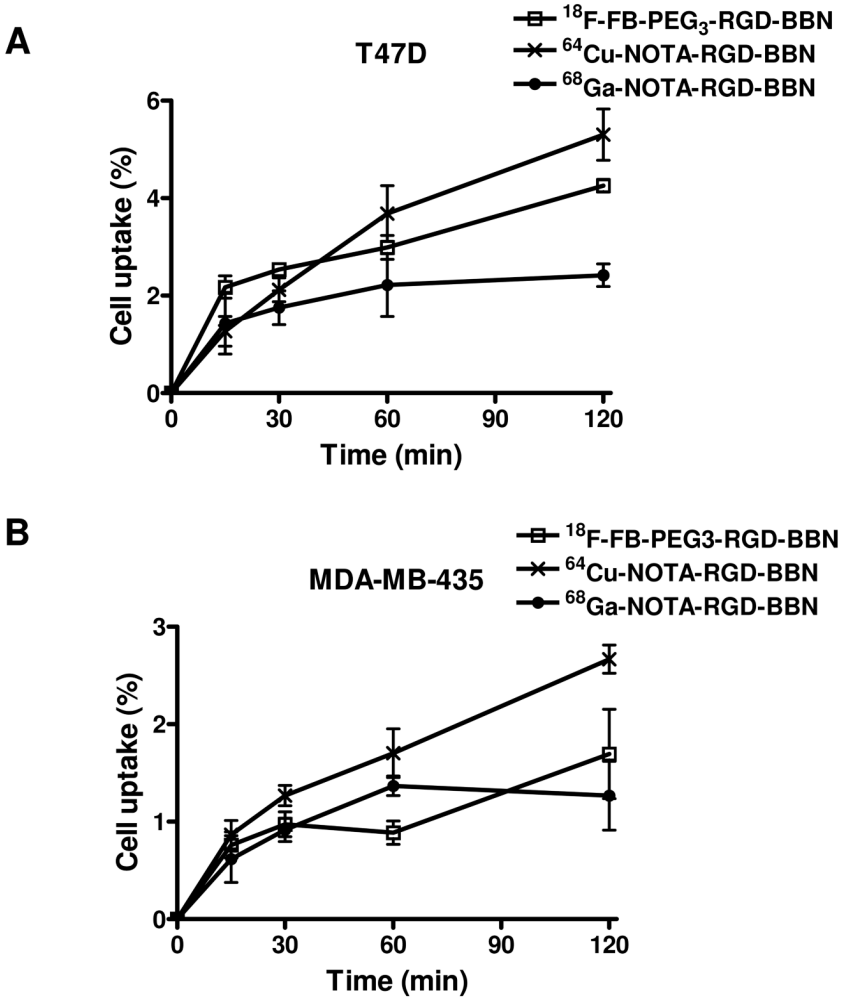

Figure 3.
Cell uptake assay of ^{18}F-FB-PEG$_3$-RGD-BBN, ^{64}Cu-NOTA-RGD-BBN and ^{68}Ga-NOTA-RGD-BBN on T47D (A) and MDA-MB-435 (B) tumor cells (means ± SD, n = 3).

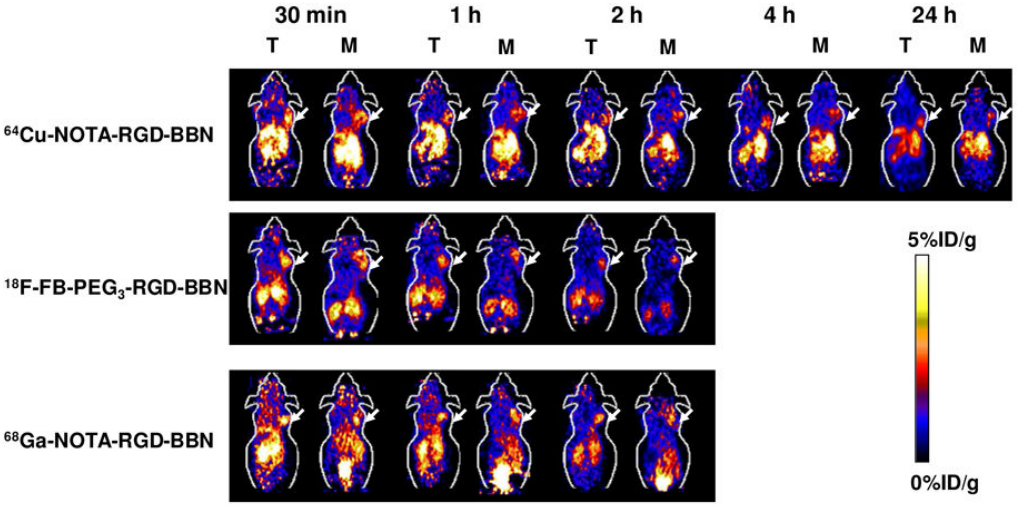

Figure 4.

Decay-corrected whole-body coronal microPET images of T47D (T) and MDA-MB-435 (M) tumor-bearing mice at 30 min, 1 h, 2 h, 4 h and 24 h after injecting 3.7~5.5 MBq (100~150 μCi) of ^{64}Cu-NOTA-RGD-BBN, ^{18}F-FB-PEG$_3$-RGD-BBN or ^{68}Ga-NOTA-RGD-BBN. Images shown are static scans of a single mouse, which is representative of the 4 mice tested in each group. Arrows indicate the presence of T47D (T) or MDA-MB-435 (M) tumors.

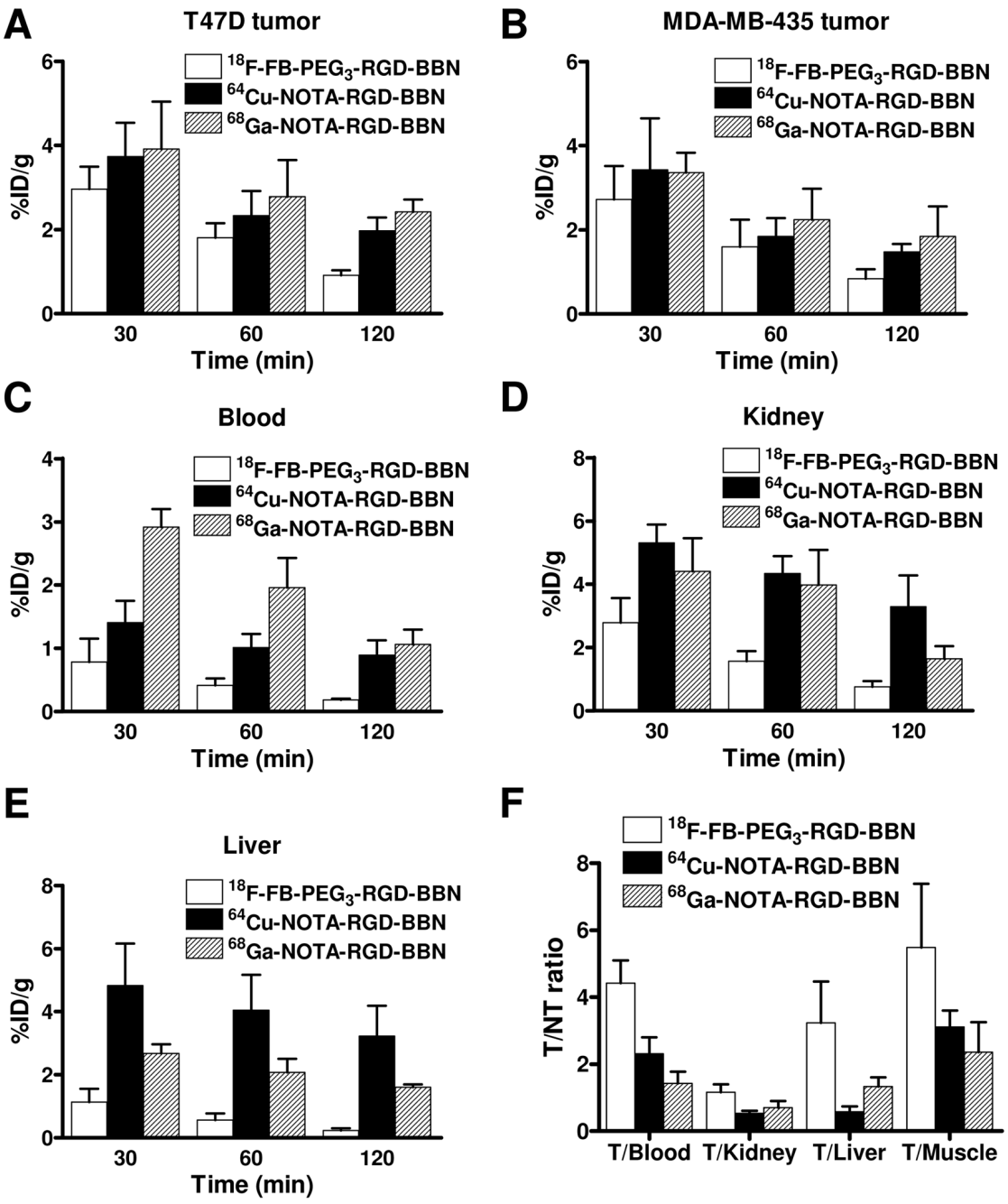

Figure 5.

(A–E) Comparison between the uptake of ^{18}F-FB-PEG$_3$-RGD-BBN, ^{64}Cu-NOTA-RGD-BBN and ^{68}Ga-NOTA-RGD-BBN in T47D tumor (A), MDA-MB-435 tumor (B), blood (C), kidneys (D), and liver (E) after injection of 3.7~5.5 MBq (100 ~150 μCi) tracer in T47D or MDA-MB-435 tumor-bearing mice (n = 4~8, mean ± SD). (F) Comparison of tumor (T) with blood, kidney, liver and muscle ratio of ^{18}F-FB-PEG$_3$-RGD-BBN, ^{64}Cu-NOTA-RGD-BBN and ^{68}Ga-NOTA-RGD-BBN at 60 min after injection of 3.7~5.5 MBq (100 ~150 μCi) tracer in T47D tumor-bearing mice (n = 4/group, mean ± SD).

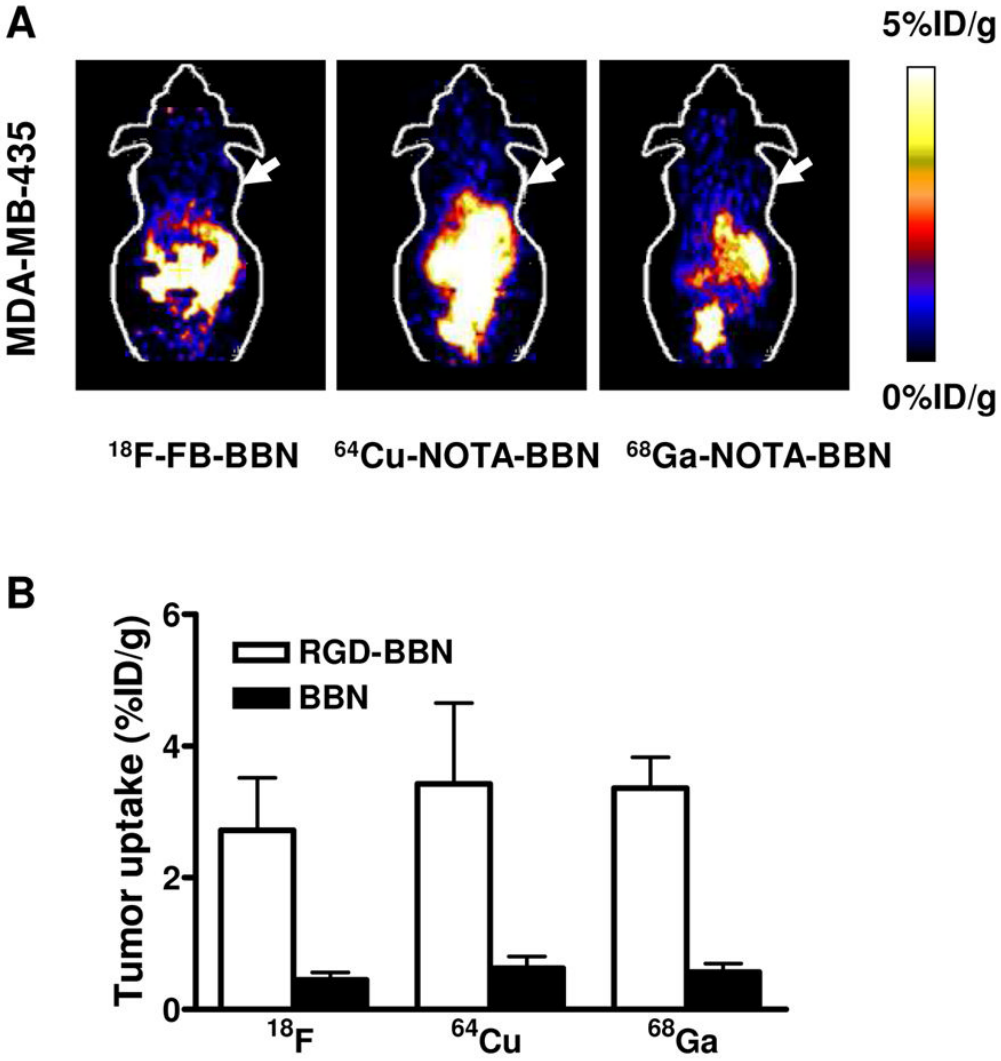

Figure 6.

(A) Decay-corrected whole-body coronal microPET images of MDA-MB-435 tumor-bearing mice at 30 min after injection of 3.7 MBq (100 μCi) ^{18}F-FB-BBN ^{64}Cu-NOTA-BBN, or ^{68}Ga-NOTA-BBN. Images shown are static scans of a single mouse, which is representative of the 3 mice tested in each group. Arrows indicate the presence of MDA-MB-435 tumors. (B) Comparison between the quantified uptake of ^{18}F/^{64}Cu/^{68}Ga labeled RGD-BBN tracers with ^{18}F/^{64}Cu/^{68}Ga labeled BBN tracers in MDA-MB-435 tumors (n = 3~4/group, mean ± SD).

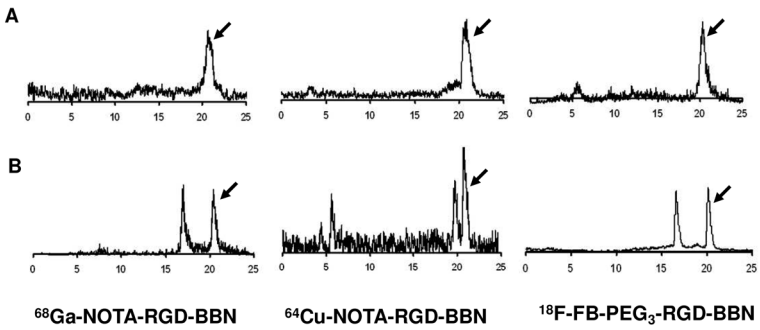

Figure 7.

(A) In vitro serum stability of ^{68}Ga-NOTA-RGD-BBN, ^{64}Cu-NOTA-RGD-BBN or ^{18}F-FB-PEG$_3$-RGD-BBN after incubating in fetal bovine serum (FBS) for 2 hour at room temperature. (B) Metabolic stability of ^{68}Ga-NOTA-RGD-BBN, ^{64}Cu-NOTA-RGD-BBN or ^{18}F-FB-PEG$_3$-RGD-BBN in mice urine at 1 h after injection (n = 2).

Table 1

Characterizations of ^{18}F-FB-PEG$_3$-RGD-BBN, ^{64}Cu-NOTA-RGD-BBN, and ^{68}Ga-NOTA-RGD-BBN.

	Receptor Affinity IC_{50} (nM)				
	Integrin $\alpha_v\beta_3$	**GRPR**	**Labeling Yield**	**Radiochemical Purity**	**Preparation Time**
^{18}F-FB-PEG$_3$-RGD-BBN	13.77 ± 1.82	73.28 ± 1.57	40~50 %	>98%	~180 min
^{64}Cu-NOTA-RGD-BBN	16.15 ± 2.77	92.75 ± 3.53	>90%	>98%	~40 min
^{68}Ga-NOTA-RGD-BBN			>90%	>98%	~45 min

Note: The IC_{50} was determined by FB-PEG$_3$-RGD-BBN and NOTA-RGD-BBN. Labeling yield of ^{18}F-FB-PEG$_3$-RGD-BBN was based on ^{18}F-SFB. Preparation time of ^{18}F-FB-PEG$_3$-RGD-BBN was determined from ^{18}F-F.

Table 2

Quantified MicroPET Imaging Data of ^{18}F-FB-PEG$_3$-RGD-BBN, ^{64}Cu-NOTA-RGD-BBN, and ^{68}Ga-NOTA-RGD-BBN in T47D and MDA-MB-435 Tumor-bearing Nude Mice (Means ± SD, n = 4~8).

	^{18}F-FB-PEG$_3$-RGD-BBN			**^{68}Ga-NOTA-RGD-BBN**		
	0.5 h	**1 h**	**2 h**	**0.5 h**	**1 h**	**2 h**
Blood	0.78 ± 0.37	0.41 ± 0.11	0.18 ± 0.02	2.91 ± 0.28	1.95 ± 0.47	1.06 ± 0.23
Liver	1.13 ± 0.43	0.56 ± 0.21	0.23 ± 0.07	2.68 ± 0.29	2.08 ± 0.43	1.60 ± 0.09
Kidney	2.77 ± 0.78	1.56 ± 0.32	0.74 ± 0.19	4.39 ± 1.05	3.96 ± 1.12	1.64 ± 0.40
Muscle	0.81 ± 0.23	0.33 ± 0.17	0.15 ± 0.05	1.33 ± 0.28	1.18 ± 0.44	0.78 ± 0.07
T47D	2.96 ± 0.53	1.81 ± 0.34	0.91 ± 0.12	3.91 ± 1.13	2.78 ± 0.87	2.42 ± 0.29
MDA-MB-435	2.72 ± 0.80	1.59 ± 0.65	0.84 ± 0.22	3.36 ± 0.47	2.24 ± 0.73	1.84 ± 0.72

	^{64}Cu-NOTA-RGD-BBN				
	0.5 h	**1 h**	**2 h**	**4 h**	**24 h**
Blood	1.40 ± 0.34	1.01 ± 0.21	0.89 ± 0.23	0.54 ± 0.20	0.36 ± 0.04
Liver	4.82 ± 1.34	4.05 ± 1.12	3.22 ± 0.97	2.76 ± 0.81	2.24 ± 0.36
Kidney	5.29 ± 0.58	4.32 ± 0.55	3.28 ± 0.99	2.95 ± 0.26	2.10 ± 0.72
Muscle	0.91 ± 0.27	0.75 ± 0.12	0.56 ± 0.33	0.40 ± 0.07	0.21 ± 0.04
T47D	3.73 ± 0.81	2.33 ± 0.59	1.97 ± 0.32	1.94 ± 0.22	1.38 ± 0.16
MDA-MB-435	3.42 ± 1.23	1.84 ± 0.44	1.47 ± 0.19	1.79 ± 0.20	1.29 ± 0.09